ASN NEURO RESEARCH ARTICLE

ASN NEURO 2(4):art:e00041.doi:10.1042/AN20100017

Astrocytic gap junctional communication is reduced in amyloid-β-treated cultured astrocytes, but not in Alzheimer's disease transgenic mice

Nancy F Cruz, Kelly K Ball and Gerald A Dienel[1]
Department of Neurology, University of Arkansas for Medical Sciences, Little Rock, AR 72205, U.S.A.

Cite this article as: Cruz NF, Ball KK and Dienel GA (2010) Astrocytic gap junctional communication is reduced in amyloid-β-treated cultured astrocytes, but not in Alzheimer's disease transgenic mice. ASN NEURO 2(4):art:e00041.doi:10.1042/AN20100017

ABSTRACT

Alzheimer's disease is characterized by accumulation of amyloid deposits in brain, progressive cognitive deficits and reduced glucose utilization. Many consequences of the disease are attributed to neuronal dysfunction, but roles of astrocytes in its pathogenesis are not well understood. Astrocytes are extensively coupled via gap junctions, and abnormal trafficking of metabolites and signalling molecules within astrocytic syncytia could alter functional interactions among cells comprising the neurovascular unit. To evaluate the influence of amyloid-β on astrocyte gap junctional communication, cultured astrocytes were treated with monomerized amyloid-β_{1-40} (1 μmol/l) for intervals ranging from 2 h to 5 days, and the areas labelled by test compounds were determined by impaling a single astrocyte with a micropipette and diffusion of material into coupled cells. Amyloid-β-treated astrocytes had rapid, sustained 50–70% reductions in the area labelled by Lucifer Yellow, anionic Alexa Fluor® dyes and energy-related compounds, 6-NBDG (a fluorescent glucose analogue), NADH and NADPH. Amyloid-β treatment also caused a transient increase in oxidative stress. In striking contrast with these results, spreading of Lucifer Yellow within astrocytic networks in brain slices from three regions of 8.5–14-month-old control and transgenic Alzheimer's model mice was variable, labelling 10–2000 cells; there were no statistically significant differences in the number of dye-labelled cells among the groups or with age. Thus amyloid-induced dysfunction of gap junctional communication in cultured astrocytes does not reflect the maintenance of dye transfer through astrocytic syncytial networks in transgenic mice; the pathophysiology of Alzheimer's disease is not appropriately represented by the cell culture system.

Key words: amyloid protein, astrocyte, connexin, dye transfer, gap junction, metabolite trafficking.

INTRODUCTION

Astrocytes are extensively linked to each other via gap junctional channels formed by Cx (connexin) proteins, Cx43, Cx30 and Cx26 (Nagy et al., 2004). These channels enable transcellular movement of fuel, metabolites, signalling molecules and electrolytes, with preferential transfer of material that is governed by molecular size, charge and connexin composition (Harris, 2007). The physiological functions of cell-to-cell transfer of energy-related metabolites within the astrocytic syncytium in brain are not well understood, but astrocytes have important roles in brain energetics (Hertz et al., 2007). Sharing among astrocytes of fuel and redox compounds and rapid elimination of metabolic by-products may be essential astrocytic responses to brain activation. For example, the astrocytes that remove glutamate and potassium from an active synaptic cleft incur an increased demand for energy that would be reduced if the neurotransmitters and electrolytes quickly diffuse into neighbouring gap junction-coupled astrocytes. Also, astrocytic uptake and

[1] To whom correspondence should be addressed (email gadienel@uams.edu).

Abbreviations: A350, Alexa Fluor® 350; A568, Alexa Fluor® 568; aCSF, artificial cerebral spinal fluid; APP, amyloid-β precursor protein; Cx, connexin; dBcAMP, dibutyryl cAMP; DCF, dichlorofluorescein; DMEM, Dulbecco's modified Eagle's medium; FBS, fetal bovine serum; GFAP, glial fibrillary acidic protein; H2DCF-DA, carboxy-dihydrodichlorofluorescein diacetate; L-LME, L-leucine methyl ester hydrochloride; 6-NBDG, 6-[N-(7-nitrobenz-2-oxa-1,3-diazol-4-yl)amino]-6-deoxyglucose; ROS, reactive oxygen species; SR101, sulforhodamine 101; STZ, streptozotocin.

dispersal of lactate among gap junction-coupled cells (Gandhi et al., 2009b) in conjunction with its discharge from perivascular endfeet that are linked to extensive gap junctional networks (Ball et al., 2007) could serve to help up-regulate blood flow in a larger volume of tissue compared with that of focally activated cells, by raising the level of lactate in the interstitial fluid near the endothelium (Gordon et al., 2008). Furthermore, release from activated astrocytes of molecules used as signals for brain imaging and spectroscopic assays (e.g. NADH, NADPH and ^{14}C- or ^{13}C-labelled metabolites of glucose or acetate) could cause underestimation of cellular redox status and metabolic rates calculated from accumulation of labelled products unless appropriately taken into account.

Alzheimer's disease is a devastating neurodegenerative disease associated with cognitive dysfunction, increased levels of amyloid-β deposits and neurofibrillary tangles in brain, oxidative stress, neuroinflammation and neuronal dysfunction (Craft, 2009; Fotuhi et al., 2009; Querfurth and LaFerla, 2010), and one of the earliest and most reliable markers for Alzheimer's disease and its progression is reduced glucose utilization in brain (Alexander et al., 2002). Astrocytic pathology is associated with Alzheimer's disease, including hypertrophy, oxidative stress, DNA damage and reduced expression of the EAAT2 glutamate transporter (Wharton et al., 2009; Simpson et al., 2010a, 2010b). Astrocytic networks may be involved in the pathophysiology, since expression of Cx43 is elevated in astrocytic processes located in amyloid plaques in brains of Alzheimer's patients (Nagy et al., 1996a), and Cx43 expression is induced in gap junction-incompetent PC12 cells after transfection with amyloid protein (Nagy et al., 1996b). Amyloid precursor protein is expressed in cultured astrocytes (Haass et al., 1991; Gegelashvili et al., 1994), and astrocytes are known to bind, take up and degrade amyloid-β (Wyss-Coray et al., 2003; Pihlaja et al., 2008; Nielsen et al., 2009). Gap junction-mediated calcium waves are elevated after transfection of PC12 cells with amyloid-β or exposure of cultured astrocytes to amyloid-β (Lynn et al. 1995; Haughey and Mattson, 2003). In ~2-year-old transgenic mice carrying the human APP (amyloid-β precursor protein) with the $APP_{717V\rightarrow F}$ mutation, gap junctional transfer of biotin was preserved, contrasting loss of dye coupling in normal mice >1-year-old (Peters et al., 2009). Taken together, the findings described above suggest that astrocytic gap junctional communication may be up-regulated in Alzheimer's disease, and, in the present study, we assessed gap junctional transport in cultured astrocytes treated with amyloid-β and in brain slices from aged transgenic mice that overexpress the human APP with the Swedish (K670N/M671L) and Indiana (V717F) mutations (Mucke et al., 2000). We report that treatment of cultured astrocytes with amyloid-β markedly reduced gap junctional transfer of six test compounds, whereas dye-transfer among astrocytes in brain slices from three regions of transgenic Alzheimer's mice is similar to that of aged littermate controls, contrasting the results of previous brain slice studies.

MATERIALS AND METHODS

Materials

DMEM (Dulbecco's modified Eagle's medium; catalogue number 12320-032), penicillin, streptomycin, Amphotericin B and trypsin were obtained from Invitrogen and FBS (fetal bovine serum) was from Hyclone. dBcAMP (dibutyryl cAMP), L-LME (L-leucine methyl ester hydrochloride), Lucifer Yellow VS (dilithium salt), NADH and NADPH were from Sigma–Aldrich. 6-NBDG {6-[N-(7-nitrobenz-2-oxa-1,3-diazol-4-yl)amino]-6-deoxyglucose}, A350 (Alexa Fluor® 350 carboxylic acid, succinimidyl ester), A568 (Alexa Fluor® 568), SR101 (sulforhodamine 101) and H2DCF-DA (carboxydihydrodichlorofluorescein diacetate) were from Invitrogen (Molecular Probes). Human amyloid-β_{1-40} (product no. A1075, formula mass 4330 Da; Sigma) was treated with hexafluoro-2-propanol to monomerize the amyloid-β (Klein, 2002); freeze-dried samples were stored at −80°C and dissolved in PBS immediately prior to use.

Astrocyte culture

Cultured astrocytes were prepared essentially as described by Hertz et al. (1998) after harvest of cells from cerebral cortex of 1-day-old albino Wistar–Hanover rats (Taconic Farms, Germantown, NY). Astrocytes were grown in T75 culture flasks with DMEM containing 5.5 mmol/l glucose, 10% FBS, 50 i.u. of penicillin and 50 μg/ml streptomycin at 37°C in humidified air containing 5% CO_2. L-LME (0.1 mmol/l), a lysosomotrophic agent that selectively destroys mononuclear cells including microglia, was included in the culture medium, and cultures were shaken by hand twice weekly to remove microglia. When confluent, the cells were trypsinized, seeded on to polylysine-coated glass coverslips, and grown to confluence in medium containing Amphotericin B (2.5 μg/ml). After the cells reached confluence, dBcAMP (0.25 mmol/l) was added to the culture medium to induce differentiation and, starting the next day, cells were maintained in a medium containing 0.25 mmol/l dBcAMP plus Amphotericin B and either 5.5 or 25 mmol/l glucose for 2–3 weeks. Then the cells were treated with 1 μmol/l of monomerized Aβ_{1-40} or vehicle for a period ranging from 2 h to 5 days. In our previous study which used identical procedures, >90% of the cells expressed the astrocyte marker GFAP (glial fibrillary acidic protein) (Gandhi et al., 2010).

Brain slices

Breeder pairs of transgenic mice (PDGF-APPSwInd, stock #004661) that contain the human APP with Swedish (K670N/M671L) and Indiana (V717F) mutations were purchased from Jackson Laboratories. The mutant mouse lines originated on a mixed C57BL/6 and DBA/2 background and were backcrossed on to the C57BL/6J background; APP expression is directed to neurons under the control of a human platelet-derived growth factor β polypeptide promoter. Amyloid plaque

deposition occurs in 50–60% of the mice at 5–7 months of age and 100% at 8–10 months of age (Mucke et al., 2000). All animal use procedures were in strict accordance with the *NIH Guide for Care and Use of Laboratory Animals* and were approved by the local Animal Care and Use Committee.

Mixed-gender heterozygous transgenic Alzheimer's mice and control littermates (n=6/group) ranging in age from 8.5 to 14 months were anaesthetized with isofluorane, decapitated, their brains were quickly removed and chilled by immersion in oxygenated, ice-cold aCSF (artificial cerebral spinal fluid) solution containing 26 mmol/l $NaHCO_3$ (pH 7.3) and 248 mmol/l sucrose, and 250 μm-thick slices were prepared as described by Moyer and Brown (1998). Coronal sections of brain were cut using a Leica VT 1000S tissue slicer, slices were incubated in oxygenated aCSF containing sucrose for 30 min at 35 °C, then for ⩾1 h at 22 °C, and transferred to an open bath perfusion chamber (Warner Instruments).

Gap junctional communication assays

Gap junctional communication among astrocytes was assayed by impaling a single cell with a micropipette containing a test compound, allowing the material to diffuse within the astrocytic network for a fixed time (2 or 5 min in cultured cells or brain slices respectively), then measuring the labelled area or counting labelled cells. Micropipettes (12–14 MΩ) were constructed from borosilicate glass using a Sutter Instruments P97 pipette puller and filled with the test solution. Most solutions contained 21.4 mmol/l KCl, 0.5 mmol/l $CaCl_2$, 2 mmol/l $MgCl_2$, 5 mmol/l EGTA, 2 mmol/l ATP, 0.5 mmol/l GTP, 2 mmol/l ascorbate, 75 mmol/l potassium gluconate [note: potassium gluconate was inadvertently omitted as a component of the pipette solution in the Materials and methods of our previous studies (Gandhi et al., 2009a, 2010)], 10 mmol/l Hepes (pH 7.2), plus a test compound, i.e. Lucifer Yellow VS [62 mmol/l or ~4% (w/v); excitation/emission maxima: 430/530 nm], a fluorescent glucose analogue 6-NBDG (20 mmol/l; 475/550 nm), A350 (5 mmol/l; 346/442 nm), A568 (5 mmol/l; 578/603 nm) or NADH or NADPH (25 mmol/l; 340/460 nm). Lucifer Yellow VS solutions for use in brain slices contained 124 mmol/l Lucifer Yellow, 10 mmol/l Hepes (pH 7.2), 48 mmol/l LiCl and 0.001% Evans Blue plus 0.01% albumin; the Evans Blue–albumin was added so that the pipette could be visualized when impaling SR101-labelled astrocytes in brain slices. For assays of 6-NBDG gap junctional transfer, efflux of the fluorescent tracer from astrocytes via glucose transporters was blocked by cytochalasin B, a glucose transport inhibitor (Speizer et al. 1985); we previously observed that glucose transporter-mediated efflux of the NBDG reduced the NBDG-labelled area by ~50% (Gandhi et al., 2009a). For these assays, the perfusion medium contained 10 μmol/l cytochalasin B, 10 mmol/l glucose (to compete for re-uptake of any tracer that leaked out of cells) and an excess level of pyruvate (10 mmol/l) was included as oxidative fuel to compensate for glucose transport blockade during dye-transfer assays. The osmolarity of each pipette solution was measured (Osmette II, Precision Systems) and adjusted to 305–320 mOsm/l with sucrose or deionized water, as appropriate.

Cultured astrocytes and slices from mouse brain were transferred to the microscope stage and perfused at 1 ml/min with freshly prepared aCSF containing 26 mmol/l $NaHCO_3$ (pH 7.3) and 10 mmol/l glucose at room temperature (~20–22 °C), and continuously bubbled with O_2/CO_2 (95/5%). Cultured astrocytes were visualized under differential interference contrast with a Nikon Eclipse E600 microscope using a Photometrics CoolSNAP ES camera (Roper Scientific) and MetaVue software (Molecular Devices). Astrocytes in slices of hippocampus, cerebral cortex and inferior colliculus slices were identified by their specific labelling by SR101(Nimmerjahn et al., 2004; Ball et al., 2007); SR101 (60 μmol/l) was included in the final aCSF solution for slice recovery. Single astrocytes were impaled with micropipettes using a MP-225 manipulator (Sutter Instruments), and tracers were diffused for 2 min into cultured astrocytes or for 5 min into astrocytes in brain slices before the micropipette was removed. Separate groups of control astrocytes grown in low glucose were assayed for dye transfer with and without pretreatment with 0.6 mmol/l octanol for 10 min to inhibit gap junctional transfer. Fluorescence was determined before (background) and immediately after diffusion of the test compound into a single astrocyte, and the areas labelled by the probes were determined with MetaVue software. Further details of the experimental procedures are described in our previous studies (Ball et al., 2007; Gandhi et al., 2009a; Gandhi et al., 2010).

Counts of the number of dye-labelled cells in brain slices were carried out as follows. The 250 μm-thick brain slices that were previously injected with Lucifer Yellow were removed from the microscope stage and immediately fixed by immersion in 4% paraformaldehyde in PBS (pH 7.4), quickly followed by mixing for 30 s, then gentle shaking for 30 min at room temperature (approx. 20 °C) before being stored at 4 °C. Prior to sectioning, the slices were rinsed in PBS, cryoprotected in 20% sucrose/PBS at 4 °C, frozen and cut into 7 μm-thick serial sections at −20 °C. Sections were mounted on SuperfrostPlus glass slides, air dried for 24 h and then stored in slide boxes at 4 °C. After the sections were coverslipped (Gelmount medium and glass coverslips), the Lucifer-Yellow-containing astrocytes were counted in each 7 μm-thick serial section using a Zeiss Axioskope2 with Zeiss Plan Neofluar objectives (×10/0.30 numerical aperture or ×20/0.50), an MTI CD72 camera and an MCID™ Imaging System (InterFocus Imaging Limited), then summed to obtain the total number of dye-labelled cells for each 250 μm-thick brain slice.

Congo Red staining of amyloid plaques

An alkaline Congo Red staining method (Puchtler et al., 1962; Wilcock et al., 2006) was used to identify amyloid plaques in the mouse brain tissue. After the Lucifer Yellow-labelled cells were counted, the coverslips were removed from the slides by soaking in water overnight, then rinsed several times to remove any remaining Gelmount. Next, the tissue sections

were soaked in deionized water for 30 s, transferred to Gill's Haematoxylin #3 (Polysciences Incorporated) for 30 s, and rinsed in tap water until the water was clear. A critical aspect of the Congo Red staining procedure was that each of the two alkaline solutions was freshly prepared and used within 15 min. The pretreatment solution was prepared by adding 2.5 ml of 1% (w/v) aqueous NaOH to 250 ml of previously prepared NaCl-saturated 80% ethanol; then the solution was mixed and filtered. The staining solution was similarly prepared by adding the NaOH to a 0.2% Congo Red (Chroma #10460) solution in 80% ethanol saturated with NaCl. The slides were first incubated for 20 min in the pretreatment solution, placed in the staining solution for 20 min, then quickly passed through three changes of absolute ethanol followed by three changes of xylene and mounted with Permount medium (Fisher Chemical). Brightfield and fluorescent images of the Congo Red-stained tissue (Puchtler and Sweat, 1965) were obtained and composite images ($\times 100$ and $\times 200$ magnification) were produced by overlaying the brightfield images with their corresponding colorized fluorescent images. The presence of amyloid plaques was confirmed by microscopic examination under cross-polarized light and demonstration of red–green birefringence (Jin et al., 2003 and references cited therein).

Assay for ROS (reactive oxygen species)/RNS (reactive nitrogen species)

H2DCF-DA is cell-membrane-permeable, cleaved by intracellular esterases and, after oxidation mediated mainly by H_2O_2 and peroxynitrite, becomes fluorescent DCF (dichlorofluorescein) (Cruthirds et al., 2005). H2DCF-DA (10 μmol/l) was added to the culture medium, cells returned to the CO_2 incubator for 30 min at 37°C, cells washed with perfusion solution and fluorescence intensity determined with Nikon E600 microscope and MetaVue software.

Statistics

All statistical analyses were performed with GraphPad Prism® software, version 5.02 (GraphPad Software). Comparisons between two groups of independent samples were made with two-tailed, unpaired *t* tests. $P<0.05$ is considered to be statistically significant. Reported values are means and vertical error bars in Figures represent 1 S.D.

RESULTS

Amyloid-β reduces Lucifer Yellow transfer through gap junctions in cultured astrocytes

Previous studies of glutamate uptake, signalling pathways and oxidative stress (Matos et al., 2008) and calcium waves (Haughey and Mattson, 2003; Chow et al., 2010) exposed cultured astrocytes to 5 μmol/l amyloid-β_{1-40} or amyloid-β_{1-42} for various time intervals; this dose is considered to be the most likely level of astrocytic exposure in Alzheimer's brain (Haughey and Mattson, 2003). A higher level of amyloid-β_{25-35} (20 μmol/l) has been used to evaluate effects on gap junctional inhibition by cytokines released by microglia (Même et al., 2006). The 5 μmol/l dose of amyloid-β_{1-42} was stated to be non-toxic to astrocytes within the 24 h (Haughey and Mattson, 2003), but even much lower doses (10 or 100 nmol/l and 1 μmol/l) of amyloid-β_{1-40} enhanced the generation of ROS and advanced glycation end-products in vascular endothelial cells grown in high (25 mmol/l) compared with low (5 mmol/l) glucose (Burdo et al., 2009). 'Aged' solutions of amyloid-β_{1-40} and amyloid-β_{1-42} in which oligomer and fibrillary aggregates of the peptide are formed are also non-toxic in the range 1–10 μmol/l, but do stimulate oxidative stress in astrocytes grown in high-glucose DMEM (Matos et al., 2008); aged amyloid also reduces free intracellular calcium levels in astrocytes, alters their morphology and increases expression of immunoreactive S100β and GFAP (Meske et al., 1998). In our initial studies, dye transfer was tested with 1, 2, 5 or 10 μmol/l of monomerized amyloid-β_{1-40}, and the lowest dose was chosen for use to minimize formation of vacuoles that were visible in cells given the highest doses. The effects of amyloid-β_{1-40} were first assessed in cultured astrocytes grown in low (5.5 mmol/l) or high (25 mmol/l) glucose because we recently found that experimental diabetes, a risk factor for Alzheimer's disease, reduces dye transfer through gap junctions in cultured astrocytes and STZ (streptozotocin)-diabetic rats (Gandhi et al., 2010), and STZ-induced diabetes also enhances cognitive deficits and expression of oxidative stress markers in presymptomatic Alzheimer's transgenic mice (Burdo et al., 2009).

In agreement with our previous results, the spread of Lucifer Yellow through gap junctions was much greater in cells grown in low (Figures 1Aa and 1Ab) compared with high (Figures 1Bd and 1Be) glucose. Treatment of both culture groups with 1 μmol/l monomerized amyloid-β for 2 h markedly reduced dye transfer compared with their respective controls (Figures 1Ac and 1Bf). This decrement averaged approx. 50–75% in astrocytes grown in low (Figure 2A) or high (Figure 2B) glucose compared with paired control cultures. Pretreatment of low-glucose control astrocytes with octanol reduced the Lucifer Yellow-labelled area by approx. 75% ($P<0.001$), from 11220 ± 4566 μm^2 (mean ± S.D.) to 2913 ± 950 μm^2, a magnitude similar to that caused by amyloid treatment. Maximal inhibition of dye transfer by amyloid-β occurred within 2 h, and increased duration of exposure to the single dose of monomerized amyloid from 2 h to 5 days did not alter the decrement (Figure 2); no attempt was made to determine the proportion of amyloid monomers, oligomers and fibrils over time. Because high glucose reduced dye transfer in control cultures and blunted the percentage change after amyloid-β treatment (Figure 2), all subsequent assays used astrocytes grown in low glucose.

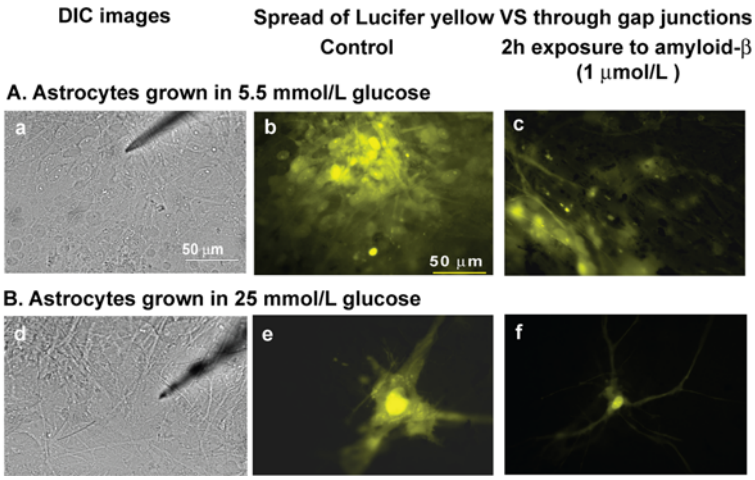

Figure 1 **Representative images of reduced Lucifer Yellow spread among astrocytes after brief exposure to amyloid-β**
Cultured astrocytes grown in (**A**) low (5.5 mmol/l) or (**B**) high (25 mmol/l) glucose-containing medium for 2–3 weeks. Cells were visualized and impaled with a micropipette (**a** and **d**), and Lucifer Yellow was diffused for 2 min into a single astrocyte in a culture treated with vehicle (**b** and **e**) or with 1 μmol/l of amyloid-β_{1-40} for 2 h prior to analysis (**c** and **f**). Scale bars indicated apply to all panels.

Amyloid-β causes modest, transient oxidative stress in astrocytes grown in low glucose

We previously identified oxidative stress as a probable causative factor in disruption of trafficking of small molecules through the astrocytic network in experimental diabetes (Gandhi et al., 2010), and amyloid-β exacerbates the generation of ROS in brain vascular endothelial cells (Burdo et al., 2009). DCF fluorescence was, therefore, assayed to evaluate the extent of amyloid-β-induced oxidative stress in the low-glucose cultures. DCF fluorescence approximately doubled after 2 h exposure to amyloid-β, but the increase did not persist at 24 h, and a slight decrement was evident at 5 days (Figure 3). The rapid onset of reduced dye transfer (Figures 1 and 2) and low, transient increase in oxidative stress with amyloid treatment (Figure 3) sharply contrast the responses of hyperglycaemic astrocytes. These cells had a rapid, progressive rise in DCF fluorescence, but there was a 3–5 day delay before the onset of inhibition of dye transfer, suggesting that other factors mediate the effects of amyloid-β on dye transfer.

Amyloid-β impairs gap junctional transfer of compounds with different size or charge

Cell-to-cell transfer of anionic dyes that are either larger (A568, 730 Da; Figures 4a and 4b) or smaller (A350, 311 Da when ionized; Figures 4c and 4d) than Lucifer Yellow VS (536 Da when ionized; Figures 1 and 2) is also markedly lowered by amyloid-β treatment. The area labelled by A568 was reduced within 2 h by amyloid-β and it persisted at 1 and 2 days (Figure 5A), whereas that labelled by A350 was statistically significantly only at day one due to lower values for the control group in the 2 day treatment group (Figure 5B). Octanol treatment of control astrocytes reduced the A568-labelled area by approx. 80%, from 7379 ± 3080 μm^2 to 1434 ± 658 μm^2 ($P<0.01$).

Diffusion within the astrocytic network of molecules related to glucose metabolism was also inhibited by amyloid-β. The area labelled by 6-NBDG (342 Da), a non-phosphorylatable uncharged fluorescent analogue of glucose (Aller et al. 1997; Speizer et al.1985) that is used to assay transport, was reduced by 40–70% after 1–2 days treatment of astrocytes with amyloid-β (Figure 6A). NADH and NADPH are phosphorylated anions involved in redox reactions in the glycolytic and pentose phosphate shunt pathways respectively. Movement of NADH (663 Da) within the astrocytic syncytium was depressed after exposure to amyloid-β for 2 h to 2 days (Figure 6B), and spreading of NADPH (723 Da) was also reduced by 24 h treatment with amyloid-β (data not shown). Octanol pretreatment of control astrocytes reduced NBDG labelling from 12816 ± 4305 μm^2 to 1153 ± 492 μm^2 ($P<0.001$) and diminished NADH labelling from 6109 ± 2873 μm^2 to 1323 ± 519 μm^2 ($P<0.01$).

Astrocytic dye transfer in brain slices from aged control and Alzheimer's mice

Because cultured astrocytes are not exposed to the same environment as cells in the aging and Alzheimer's model mouse brain, Lucifer Yellow transfer was also assayed in 8.5–14-month-old transgenic mice that overexpress mutant human APP and in age-matched littermate controls. Mice with the mutant APP were identified by genotyping, and amyloid plaque formation was verified in all animals designated as 'Alzheimer's mice' after the dye-labelled cells were counted. Congo Red-stained amyloid plaques were

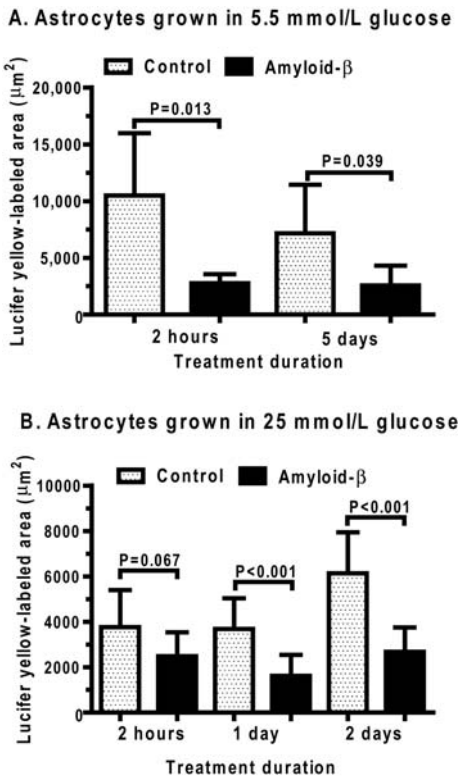

Figure 2 Amyloid-β treatment reduces gap junctional spreading of Lucifer Yellow in low- and high-glucose astrocyte cultures
Cultured astrocytes grown in low (**A**) or high (**B**) glucose were treated with 1 μmol/l monomerized amyloid-β_{1-40} or vehicle for up to 5 days prior to assay of the Lucifer Yellow-labelled area (see Figure 1). The number of injected cells for the control and amyloid-β-treated groups respectively, at each time point are as follows: (**A**) 2 h, n=6, 5; 5 days, n=5, 6; (**B**) 2 h, n=9, 9; 1 day, n=10, 11; 2 days, n=14, 14.

readily detected in parenchyma and perivascular space in hippocampus (Figure 7A) and cerebral cortex (Figure 7B) of transgenic mice. Some perivascular staining, but not Congo

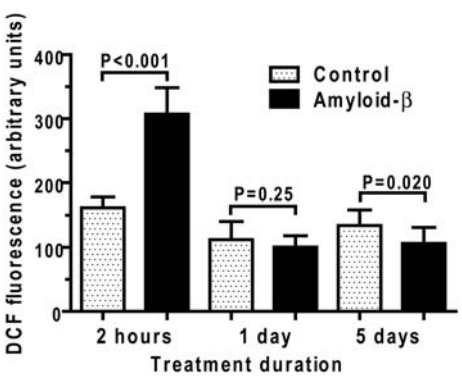

Figure 3 DCF fluorescence in amyloid-β-treated astrocytes
Cultured astrocytes grown in low-glucose medium for 2–3 weeks were treated with 1 μmol/l monomerized amyloid-β_{1-40} or vehicle for up to 5 days. The number of injected cells for the control and amyloid-treated groups respectively at each time point are as follows: 2 h, n=16, 16; 1 day, n=11, 12; 5 days, n=10, 10.

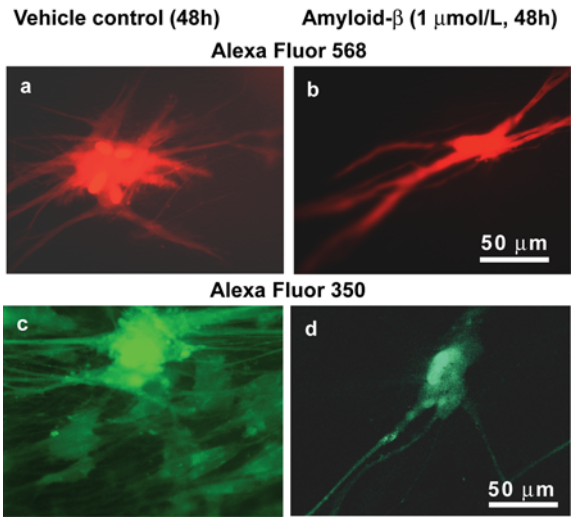

Figure 4 Representative images of impaired Alexa Fluor® dye spread among astrocytes after brief exposure to amyloid-β
Cultured astrocytes grown in low-glucose medium for 2–3 weeks were treated with vehicle (**a** and **c**) or 1 μmol/l monomerized amyloid-β_{1-40} for 48 h (**b** and **d**) prior to assay of dye spreading after diffusion of tracer into a single cell. Scale bars shown apply to all panels.

Red-stained plaques in parenchyma, was detected in the inferior colliculus of APP mice (Figure 7C). However, this does not rule out the presence of amyloid plaques in this structure, since a higher-sensitivity method to detect immunoreactive amyloid protein was not used. Because Congo Red can also bind to non-amyloid substances and some small red-stained areas (data not shown) were observed in white matter and in control brain, Congo Red-stained plaques were also examined by polarized microscopy; the plaques exhibited red–green birefringence (data not shown) which is characteristic of amyloid deposits (Jin et al., 2003).

Astrocytes in slices of hippocampus (Figure 8a), cerebral cortex and inferior colliculus from mixed-gender control and Alzheimer's mice were identified as SR101-positive cells (Nimmerjahn et al., 2004; Ball et al., 2007), then a single astrocyte was impaled with a micropipette (Figure 8b) containing Lucifer Yellow VS (Figure 8c), and the dye was allowed to diffuse into the astrocytic syncytium for 5 min. Many dye-labelled astrocytes were readily detected in the 7 μm-thick serial sections of the 250 μm-thick slices from all three brain structures of Alzheimer's and control mice. The labelling patterns differed in the three brain structures (Figures 8d–8f), although there was also some within-structure variation due to the exact location of the impaled astrocyte in each structure. In the hippocampus, labelling derived from impaled astrocytes located near the pyramidal neuronal layer was prominent and most dense in the astrocytes along the pyramidal neuronal layer, with labelled cells above and below the pyramidal layer (Figure 8d). In contrast, dye spread among astrocytes in the cerebral cortex caused labelling of cells in an approximate circular pattern around the impaled cell (Figure 8e). Astrocytic labelling in the

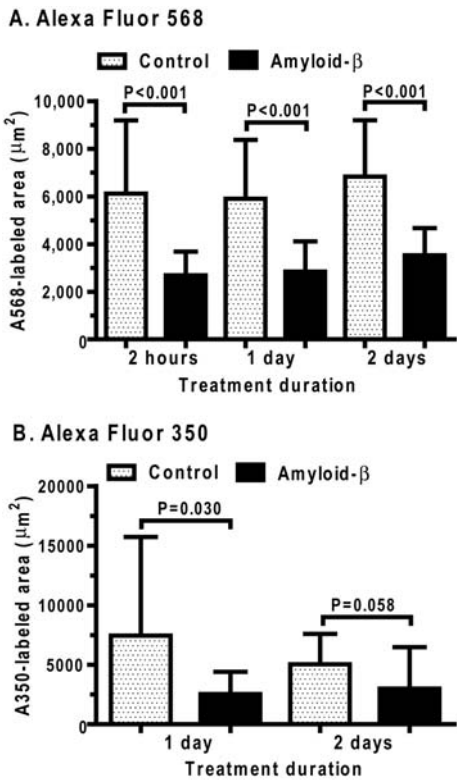

Figure 5 Amyloid-β impairs trafficking of large and small Alexa Fluor® dyes

Cultured astrocytes grown in low-glucose medium for 2–3 weeks were treated with 1 μmol/l monomerized amyloid-β_{1-40} or vehicle for up to 2 days prior to assay of the labelled area by (**A**) A568 or (**B**) A350 that was diffused for 2 min into a single cell. The number of injected cells for the control and amyloid-treated groups respectively, at each time point are as follows: (**A**) 2 h, n=37, 41; 1 day, n=61, 61; 2 days, 31, 48; (**B**) 2 h, n=13, 16; 2 days, n=16, 19.

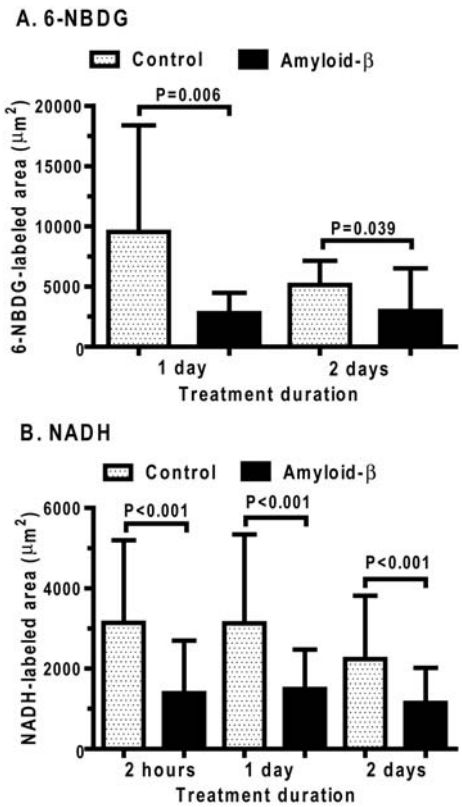

Figure 6 Amyloid-β reduces syncytial distribution of energy-related molecules

Cultured astrocytes grown in low-glucose medium for 2–3 weeks were treated with 1 μmol/l monomerized amyloid-β_{1-40} or vehicle for up to 2 days prior to assay of the labelled area by (**A**) 6-NBDG, a fluorescent glucose analogue (molecular mass, 342 Da) or (**B**) NADH (molecular mass, 663 Da) which was diffused into a single astrocyte. The number of injected cells for the control and amyloid-treated groups respectively, at each time point are as follows: (**A**) 1 day, n=12, 16; 2 days, n=16, 19; (**B**) 2 h, n=37, 41; 1 day, 61, 61; 2 days, n=30, 48.

inferior colliculus in the thin sections tended to be scattered (Figures 8f), but most of the 250 μm-thick sections (data not shown) had a radial labelling pattern that extended from the injected cell towards the meningeal boundary, as we previously observed (Ball et al., 2007).

The total number of dye-labelled cells was quite variable in both control and APP mice, ranging from a low of approx. ten, up to several thousand coupled cells, with no statistically significant differences in the number of dye-labelled cells in control and APP mice for any of the three brain regions (Figure 9). When data from all slices from all animals were plotted as a function of age, there were no obvious age-dependent trends over the relatively narrow range of ages of mice used in the present study; control and APP mice had variable and overlapping numbers of dye-labelled cells (Figure 10). Unfortunately, the number of APP mice available for this study was limited by breeding problems that persisted over approx. 2 years of the funding period; this issue reduced the number of ages and number of regional brain slices that were assessed, as well as the scope of planned work which included evaluation of gap junctional trafficking of endogenous metabolites and local rates of glucose utilization during brain activation.

DISCUSSION

Discordant results in tissue culture and brain slices: complications can arise from severe hyperglycaemia

The major finding of the present study is that exposure of cultured cerebral cortical astrocytes to low-dose monomerized amyloid-β_{1-40} markedly impaired transfer of material within the syncytial network, but dye transfer was unaffected in aged transgenic mice overexpressing amyloid protein. In low-glucose cultures, amyloid-β treatment affected transcellular diffusion of six anionic and neutral compounds with

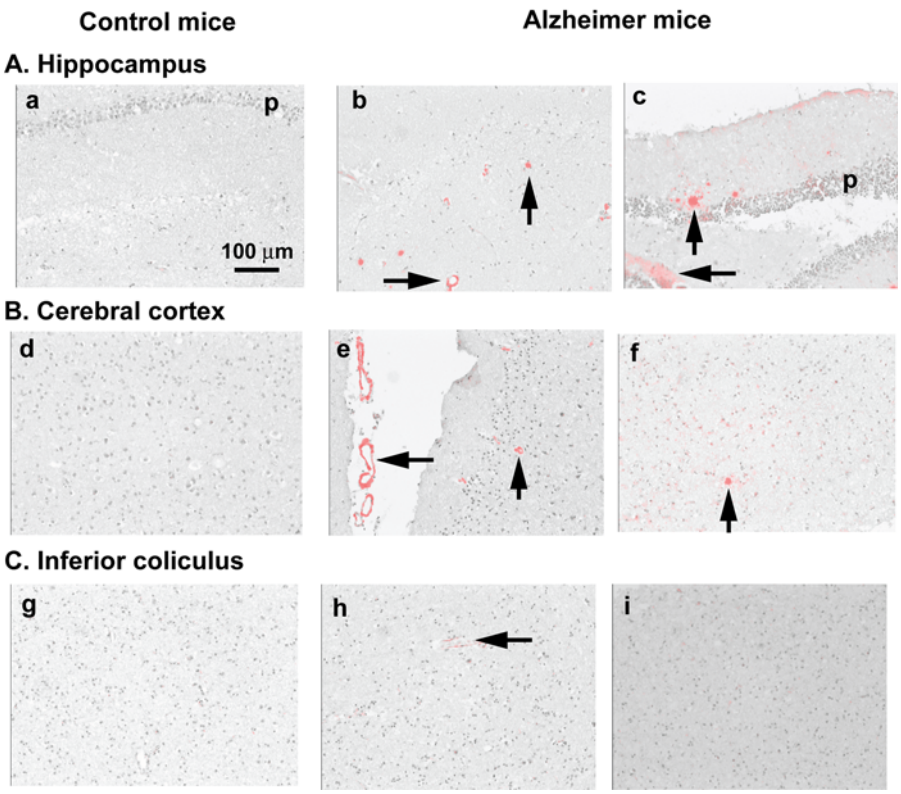

Figure 7 **Amyloid deposits in parenchyma and perivascular space of Alzheimer's transgenic mice**
Brain sections from anterior dorsal hippocampus (**A**), anterior cerebral cortex (**B**) and inferior colliculus (**C**) from each of the aged control and transgenic mice were stained with haematoxylin and Congo Red after dye-labelled cells were counted. Control mice (a, d and g) had no amyloid plaques, whereas plaques (vertical arrows: b, c, d and f) were present in hippocampus and cerebral cortex of all transgenic mice. Perivascular amyloid deposits (horizontal arrows) are visible in cross-sectional views of blood vessels (b, e and h). The horizontal arrow in (c) indicates an artefact owing to folded tissue. Two representative images from each brain region from different transgenic mice are illustrated for each brain region. Panel (e) is close to the midline of the brain and perivascular labelling is in the meninges between the two hemispheres; in hippocampus panels (a) and (c), 'p' denotes the pyramidal neuronal layer. The scale bar shown applies to all panels.

molecular masses ranging from approx. 350 to 700 Daltons; it had a rapid onset (within 2 h), it was accompanied by modest, transient oxidative stress and the inhibition was sustained for at least 5 days after a single treatment (Figures 1–6). Because transcellular movement of NADH, NADPH and 6-NBDG were reduced by amyloid treatment, signals used to monitor redox status and glucose transport and utilization are affected and could influence metabolic studies, particularly in cultured astrocytes. Amyloid-β depressed gap junctional trafficking to a similar level in high- and low-glucose cultures, but those grown in high glucose had a smaller overall percentage decrease (Figures 1 and 2) owing to reduced dye transfer among the severely hyperglycaemic cells (Gandhi et al., 2010, Thi et al., 2010).

Diabetes is a risk factor that exacerbates pathophysiological changes in Alzheimer's transgenic mice and cultured cells, with synergistic interactions that increase generation of advanced glycation products and ROS and diminish cognitive function (Burdo et al., 2009). STZ-diabetic rats have elevated levels of amyloid-β in brain (Li et al., 2007; Liu et al., 2008), but, to our knowledge, gap junctional trafficking has not been evaluated in a diabetic-Alzheimer's rodent model. Interpretation of the inhibitory effects on glucose metabolic pathways, glutamate uptake, signalling pathways, gap junctional communication and other processes that have been ascribed to amyloid peptides in other studies are complicated by the use of astrocytes that were cultured in media containing 25–40 mmol/l glucose (Parpura-Gill et al., 1997; Même et al., 2006; Matos et al., 2008; Allaman et al., 2010) or by lack of information regarding medium glucose concentration (Meske et al., 1998; Haughy and Mattson, 2003; Chow et al., 2010). A glucose level of 25 mmol/l is approx. 10-fold greater than that in normal rat brain, and it exceeds that in diabetic rat brain by 3.6-fold; it is well known that prolonged hyperglycaemia causes oxidative stress, glycation reactions and sorbitol production (Gandhi et al., 2010 and references cited therein). In fact, astrocytes grown in high-glucose medium oxidize glucose and lactate at a rate half that of those grown in low glucose (Abe et al., 2006). Exposure to amyloid peptides and amyloid aggregates has deleterious consequences for cultured astrocytes and neurons, but the possibility of synergistic interactions of amyloid treatment with severely

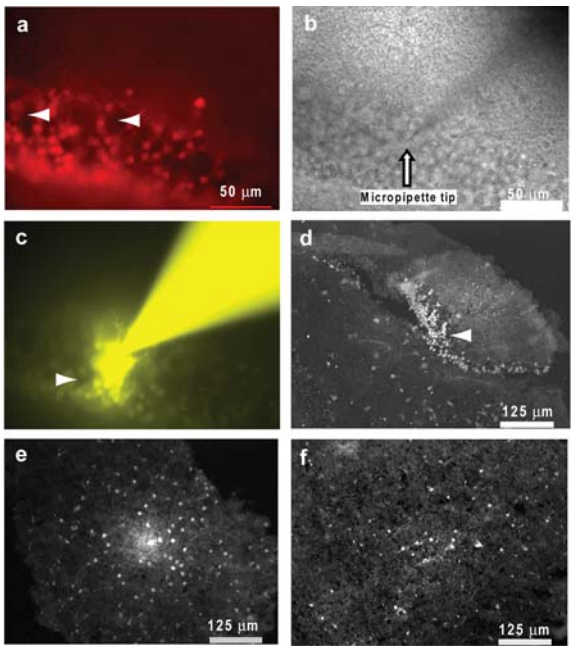

Figure 8 Representative images of Lucifer Yellow diffusion among astrocytes in slices from three brain regions of aged Alzheimer's transgenic mice

Brain slices (250 μm thick) were prepared from hippocampus (**a**–**b**), cerebral cortex (**e**) and inferior colliculus (**f**) of aged Alzheimer's transgenic mice. Astrocytes were identified as sulforhodamine-positive cells (**a**), then impaled with a micropipette (**b**) containing Lucifer Yellow that was allowed to diffuse into the astrocyte for 5 min (**c**). Then the sections were immediately fixed, cut into 7 μm-thick serial sections and dye-labelled cells counted in each section from each slice. Fluorescence images of typical sections are shown for each brain region to illustrate the different patterns of dye-labelled cells (bright spots) derived from impaling an astrocyte near the pyramidal neuronal layer in the hippocampus (**d**), or an astrocyte in cerebral cortex (**e**) and inferior colliculus (**f**). Arrowheads in (**a**), (**c**) and (**d**) denote dark spaces corresponding to unlabelled neuronal cell bodies. The scale bar in (**a**) also applies to (**c**).

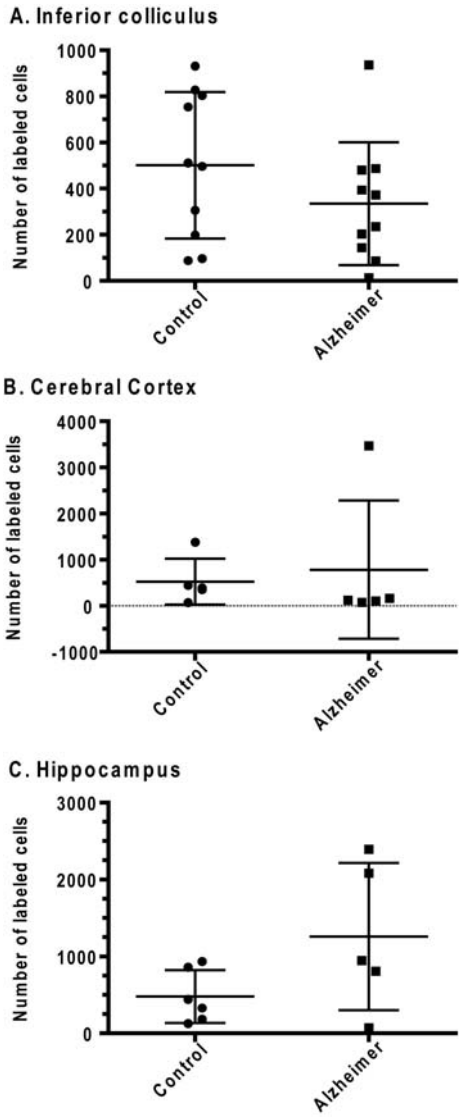

Figure 9 Dye transfer in brain regions in slices from aged control and Alzheimer's mice

Total number of Lucifer-Yellow-labelled cells in three brain regions (**A**, **B** and **C**) from control and Alzheimer's transgenic mice ranging in age from 8.5 to 14 months. Each point represent one brain slice; 1–3 slices were obtained from each region of six control and six transgenic mice. The number of slices for inferior colliculus, cerebral cortex and hippocampus respectively, were: controls, 10, 5, 6; transgenic, 10, 5, 5. Note that two of the control cortical slices had similar numbers of labelled cells and the values in the Figure overlap. There were no statistically significant differences between the control and experimental groups in each region.

diabetic conditions that potentiate damage needs to be examined and clarified.

Influence of inflammation, calcium level and age or brain region on dye coupling.

Rapid and sustained down-regulation of dye spread among cultured astrocytes by amyloid-β_{1-40} contrasts the results of Même et al. (2006), who found no effect of amyloid-β_{25-35} on Lucifer Yellow diffusion through gap junctions in scrape-load assays; this smaller peptide did, however, enhance the inhibitory effects of cytokines released from LPS (lipopoly-saccharide)-activated microglia that were grown in mixed cultures with astrocytes (38% microglia). Notably, non-activated mixed cultures had similar dye-labelled areas as astrocyte cultures (Même et al., 2006), suggesting that any microglia that remained in our non-activated astrocyte cultures (>90% are GFAP-positive cells) are unlikely to have contributed to dye-transfer inhibition.

High calcium levels can close gap junctions, but the physiological relevance of the level required is not clear (Rozental et al., 2001). Amyloid peptides are thought to form calcium channels in the astrocytic membrane, giving rise to intracellular calcium signals and oxidative stress due to activation of NADPH oxidase (Abramov et al., 2004). Exposure of astrocytes to amyloid-β_{1-42} increases intracellular calcium concentration, as well as the amplitude, velocity and travel distance of mechanically induced calcium waves (Haughey and Mattson, 2003). Acute dosing with amyloid-β_{1-40} causes

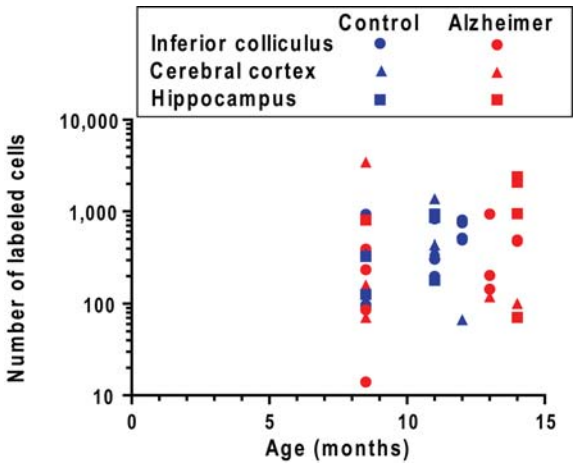

Figure 10 Dye transfer as function of age in control and Alzheimer's mice
Values from all structures and all slices in Figure 9 are plotted as a function of age of the animal.

time-delayed spontaneous calcium waves (Chow et al., 2010), whereas various 'aged' amyloid peptide preparations reduce intracellular calcium level in a dose- and time-dependent manner (Meske et al., 1998). In our gap junction assay procedure, impaling an astrocyte would initiate calcium waves, but dye spread does occur in control and amyloid-treated cells, and the contribution of calcium to differential channel closure in these two groups of cells, if any, is not clear. Other factors, such as amyloid-induced alterations in membranes that may modify Cx function or level, altered signalling cascades, and shifts in gene expression, may also be involved at different times after addition of monomerized amyloid-β_{1-40}. The basis for the inhibitory bioactivity of amyloid-β on gap junctions in cultured astrocytes remains to be established in future studies.

Surprisingly, the robust blockade of dye transfer within networks of amyloid-β-treated cultured cerebral cortical astrocytes did not occur in cerebral cortex, hippocampus or inferior colliculus of APP-transgenic mice (Figures 8–10). These findings indicate that: (i) amyloid treatment alone is not sufficient to represent the more complex pathophysiology of astrocytic networks in the aged APP mouse brain, (ii) there may be compensatory responses that maintains syncytial connectivity in APP mouse brain, beyond the localized up-regulation of immunoreactive Cx43 observed in human amyloid plaques (Nagy et al., 1996a) and (iii) global compared with regional differences do not explain the different results in cultured cells and brain slices. Discordant results in tissue culture-brain slice assays were not, however, an issue in our recent study of experimental diabetes, in which both model systems exhibited reduced dye coupling and increased oxidative stress in spite of large differences in glucose level, time of exposure to high glucose and syncytial size (Gandhi et al., 2010). In the diabetic rat literature, plasma and brain glucose levels rise an average of approx. 3-fold to 27 and 7 mmol/l respectively (Gandhi et al., 2010), and the normal adult rat inferior colliculus has up to approx. 12000 dye-coupled cells compared with 10–20 cells in cultured cortical astrocytes (Ball et al., 2007 and references cited therein). In the present study, most slices from aged control and APP mice had >100 coupled cells, with an average regional number of dye-coupled cells ranging from approx. 300 to 1100 (Figures 9 and 10), values that are much lower than in young adult rats. Peters et al. (2009) recently characterized properties of astrocytes in aged Alzheimer's transgenic mice and observed modest syncytial labelling (≤114 cells) with biocytin [molecular mass 372 Da; diffused into cells for 20 min via patch clamp pipettes containing a 0.5% (13 mmol/l) solution] in young control mice and aged Alzheimer's mice, with no apparent relationship to distance of the injected cell from an amyloid plaque. In contrast, their aged control mice (>12 months) had no detectable networks in cerebral cortex and only three out of 20 cells in hippocampal slices were coupled. The reasons for lower coupling in aged APP mice and very poor dye transfer in their aged controls are not known. Conceivably, differences might arise from the genotype of the mice used in the studies by Peters et al. (2009) and by us, or from age-related differences in transfer of biocytin compared with Lucifer Yellow VS. Also, it is important to recognize that changes in transfer of a specific dye do not necessarily predict the passage of other compounds. For example, when diffused into single astrocytes in culture or in brain slices, hexose-6-phosphates are very poorly transferred through gap junctions compared with various fluorescent dyes that were used as internal permeant standards in the same assays (Gandhi et al., 2009a). Our dye-transfer assays used high concentrations of Lucifer Yellow VS to maximize sensitivity for detection of astrocytic coupling and to more easily count labelled cells in brain slices, since dye-labelled nuclei are more prominent with Lucifer Yellow VS compared with Lucifer Yellow CH. Dye leakage from impaled cells is unlikely to cause significant labelling due to washout via the perfusion solution and to negligible labelling by extracellular membrane-impermeant dye; labelling of brain slices caused by micropipette insertion or by damaging an impaled cell is very low. Also, in our previous studies, Lucifer Yellow labelling of cultured astrocytes located at some distance from the scrape-load site was negligible (Gandhi et al., 2010), and efflux of Lucifer Yellow (and, by inference, uptake from extracellular sources) from pre-loaded cells was not detectable unless cells were exposed to a divalent-cation-deficient medium to open 'hemichannel' or pannexin pores (Gandhi et al., 2009a). To summarize, astrocytic gap junctional communication in different model systems for Alzheimer's disease varies considerably, and *in vivo* responses may be influenced by amyloid burden, age, local cytokine level, oxidative stress and other unidentified factors.

Metabolite trafficking and brain imaging in Alzheimer's disease

The hippocampus and cerebral cortex are involved in memory and cognition, and these brain regions are, therefore,

commonly used as experimental systems for studies of Alzheimer's disease and loss of higher brain function. However, other brain systems are also involved in the disease, and, for example, Alzheimer's patients have hearing impairment (Palmer et al., 1999) and abnormal auditory evoked potentials and latency responses associated with midbrain–brainstem auditory processing (O'Mahony et al., 1994). The inferior colliculus, an auditory structure with the highest metabolic rate in brain (Sokoloff et al., 1977), has amyloid plaques (Sinha et al. 1993) and a lower level of cytochrome oxidase (Gonzalez-Lima et al. 1997), indicating a reduced capacity for oxygen utilization. Dye transfer was therefore examined in these three brain structures after testing a variety of fluorescent compounds in tissue culture. Assay of local rates of glucose utilization using [^{18}F]FDG-PET ([^{18}F]fluorodeoxyglucose-positron emission tomography) has been an important tool to evaluate the progression and treatment of Alzheimer's disease (Alexander et al., 2002), and magnetic resonance spectroscopic studies using [^{13}C]glucose are increasingly used to study brain diseases because fluxes of labelled carbon into different pathways can be evaluated. Progressive mitochondrial dysfunction and impaired oxidative metabolism of glucose in brain of Alzheimer's patients (Gibson et al., 2008) would increase lactate production and release from brain. Incomplete retention of labelled lactate and other diffusible compounds in regions of interest during metabolic assays would contribute to underestimation of glucose utilization rates determined with labelled glucose compared with fluorodeoxyglucose, the products of which are phosphorylated and trapped intracellularly. Also, increases in glycolytic flux in the early stages of the disease to compensate for energy deficits arising from mitochondrial damage could give the false impression that cellular function is normal, when, in fact, cellular damage is evolving, and by the time glucose utilization rates fall, the damage may be irreversible or reflect cell death. For these reasons, it is particularly important to use different approaches to evaluate functional metabolism in diseased brain. Our previous studies have focused on evaluating the cellular contributions to discordant images of auditory activation in rats derived from labelled glucose and deoxyglucose (Cruz et al., 2007). The results strongly support the conclusions that: (i) lactate release from activated brain accounts for most of the 'missing' glucose metabolites, (ii) lactate transporters and astrocytic gap junctional trafficking are involved in this process and (iii) release of some glucose, lactate, other metabolites and amyloid-β occurs by lymphatic drainage from the inferior colliculus through perivascular channels to the cervical lymph nodes (Dienel and Cruz, 2008; Gandhi et al., 2009a, 2009b; Ball et al., 2010). Amyloid deposits accumulate in the parenchyma and perivascular space in brain of animals with Alzheimer traits (e.g. Figure 7) and in Alzheimer's patients, and partial blockade of perivascular fluid flow is postulated to contribute to the pathophysiology of Alzheimer's disease (Carare et al., 2008; Weller et al., 2008). In diabetic patients, cerebrovascular disease and thickening of the extracellular matrix would exacerbate this condition by impairing vascular elasticity, diminishing arterial pulsations that power perivascular fluid flow and reducing the distribution within brain of fuel, signalling molecules, neurotransmitters and electrolytes, as well as clearance of metabolic by-products from activated regions. Further work is necessary to: (i) evaluate astrocytic networks in aged control brain compared with aged Alzheimer's brain and (ii) determine whether changes in metabolite trafficking and functions of the neurovascular unit (i.e. interactions of astrocytes, neurons and endothelial cells involved in cerebrovascular and metabolic regulation) influence the outcome and interpretation of brain imaging and spectroscopic studies in Alzheimer's patients.

ACKNOWLEDGEMENTS

We thank Dr Murat Gokden (Department of Pathology, University of Arkansas for Medical Sciences) for suggesting and carrying out the birefringence assays of Congo Red-stained amyloid plaques.

FUNDING

This work was supported by the Alzheimer's Foundation [grant number IIRG-06-26022] and the National Institute of Neurological Disorders and Stroke [grant numbers NS038230, NS47546]. The content is solely the responsibility of the authors and does not necessarily represent the official views of the National Institute of Neurological Disorders and Stroke or the National Institutes of Health.

REFERENCES

Abe T, Takahashi S, Suzuki N (2006) Oxidative metabolism in cultured rat astroglia: effects of reducing the glucose concentration in the culture medium and of D-aspartate or potassium stimulation. J Cereb Blood Flow Metab 26:153–160.

Abramov AY, Canevari L, Duchen MR (2004) Calcium signals induced by amyloid β peptide and their consequences in neurons and astrocytes in culture. Biochim Biophys Acta 1742:81–87.

Alexander GE, Chen K, Pietrini P, Rapoport SI, Reiman EM (2002) Longitudinal PET evaluation of cerebral metabolic decline in dementia: a potential outcome measure in Alzheimer's disease treatment studies. Am J Psychiatry 159:738–745.

Allaman I, Gavillet M, Bélanger M, Laroche T, Viertl D, Lashuel HA, Magistretti PJ (2010) Amyloid-β aggregates cause alterations of astrocytic metabolic phenotype: impact on neuronal viability. J Neurosci 30:3326–3338.

Aller CB, Ehmann S, Gilman-Sachs A, Snyder AK (1997) Flow cytometric analysis of glucose transport by rat brain cells. Cytometry 27:262–268.

Ball KK, Gandhi GK, Thrash J, Cruz NF, Dienel GA (2007) Astrocytic connexin distributions and rapid, extensive dye transfer via gap junctions in the inferior colliculus: implications for [^{14}C]glucose metabolite trafficking. J Neurosci Res 85:3267–3283.

Ball KK, Cruz NF, Mrak RE, Dienel GA (2010) Trafficking of glucose, lactate, and amyloid-β from the inferior colliculus through perivascular routes. J Cereb Blood Flow Metab 30:162–176.

Burdo JR, Chen Q, Calcutt NA, Schubert D (2009) The pathological interaction between diabetes and presymptomatic Alzheimer's disease. Neurobiol Aging 30:1910–1917.

Carare RO, Bernardes-Silva M, Newman TA, Page AM, Nicoll JA, Perry VH, Weller RO (2008) Solutes, but not cells, drain from the brain parenchyma along basement membranes of capillaries and arteries: significance for cerebral amyloid angiopathy and neuroimmunology. Neuropathol Appl Neurobiol 4:131–144.

Chow SK, Yu D, Macdonald CL, Buibas M, Silva GA (2010) Amyloid β-peptide directly induces spontaneous calcium transients, delayed intercellular calcium waves and gliosis in rat cortical astrocytes. ASN NEURO 2(1): art:e00026.doi:10.1042/AN20090035

Craft S (2009) The role of metabolic disorders in Alzheimer disease and vascular dementia: two roads converged. Arch Neurol 66:300–305.

Cruthirds DL, Saba H, MacMillan-Crow LA (2005) Overexpression of manganese superoxide dismutase protects against ATP depletion-mediated cell death of proximal tubule cells. Arch Biochem Biophys. 437:96–105.

Cruz NF, Ball KK, Dienel GA (2007) Functional imaging of focal brain activation in conscious rats: impact of [^{14}C]glucose metabolite spreading and release. J Neurosci Res 85:3254–3266.

Dienel GA, Cruz NF (2008) Imaging brain activation: simple pictures of complex biology. Ann N Y Acad Sci 1147:139–170.

Fotuhi M, Hachinski V, Whitehouse PJ (2009) Changing perspectives regarding late-life dementia. Nat Rev Neurol 5:649–658.

Gandhi GK, Cruz NF, Ball KK, Theus SA, Dienel GA (2009a) Selective astrocytic gap junctional trafficking of molecules involved in the glycolytic pathway: impact on cellular brain imaging. J Neurochem 110:857–869.

Gandhi GK, Cruz NF, Ball KK, Dienel GA (2009b) Astrocytes are poised for lactate trafficking and release from activated brain and for supply of glucose to neurons. J Neurochem 111:522–536.

Gandhi GK, Ball KK, Cruz NF, Dienel GA (2010) Hyperglycaemia and diabetes impair gap junctional communication among astrocytes. ASN NEURO2(2):art:e00030. doi:10.1042/AN20090048

Gegelashvili G, Schousboe A, Linnemann D (1994) Expression of amyloid precursor protein (APP) in rat brain and cultured neural cells. Int J Dev Neurosci. 12:703–708.

Gibson GD, Ratan RR, Beal MF (2008) Mitochondria and oxidative stress in neurodegenerative disorders. Ann NY Acad Sci 1147:1–412.

Gonzalez-Lima F, Valla J, Matos-Collazo S (1997) Quantitative cytochemistry of cytochrome oxidase and cellular morphometry of the human inferior colliculus in control and Alzheimer's patients. Brain Res 752:117–126.

Gordon GR, Choi HB, Rungta RL, Ellis-Davies GC, MacVicar BA (2008) Brain metabolism dictates the polarity of astrocyte control over arterioles. Nature 456:745–749.

Haass C, Hung AY, Selkoe DJ (1991) Processing of β-amyloid precursor protein in microglia and astrocytes favors an internal localization over constitutive secretion. J Neurosci 11:3783–3793.

Harris AL (2007) Connexin channel permeability to cytoplasmic molecules. Prog Biophys Mol Biol 94:120–143.

Haughey NJ, Mattson MP (2003) Alzheimer's amyloid β-peptide enhances ATP/gap junction-mediated calcium-wave propagation in astrocytes. NeuroMolecular Med 3:173–180.

Hertz L, Peng L, Lai JC (1998) Functional studies in cultured astrocytes. Methods 16:293–310.

Hertz L, Peng L, Dienel GA (2007) Energy metabolism in astrocytes: high rate of oxidative metabolism and spatiotemporal dependence on glycolysis/glycogenolysis. J Cereb Blood Flow Metab 27:219–249.

Jin LW, Claborn KA, Kurimoto M, Geday MA, Maezawa I, Sohraby F, Estrada M, Kaminksy W, Kahr B (2003) Imaging linear birefringence and dichroism in cerebral amyloid pathologies. Proc Natl Acad Sci USA. 100:15294–15298.

Klein WL (2002) Aβ toxicity in Alzheimer's disease: globular oligomers (ADDLs) as new vaccine and drug targets. Neurochem Int 41, 345–352.

Li ZG, Zhang W, Sima AA (2007) Alzheimer-like changes in rat models of spontaneous diabetes. Diabetes 56:1817–1824.

Liu Y, Liu H, Yang J, Liu X, Lu S, Wen T, Xie L, Wang G (2008) Increased amyloid β-peptide (1–40) level in brain of streptozotocin-induced diabetic rats. Neuroscience 153:796–802.

Lynn BD, Marotta CA, Nagy JI (1995) Propagation of intercellular calcium waves in PC12 cells overexpressing a carboxy-terminal fragment of amyloid precursor protein. Neurosci Lett 199:21–24.

Matos M, Augusto E, Oliveira CR, Agostinho P (2008) Amyloid-β peptide decreases glutamate uptake in cultured astrocytes: involvement of oxidative stress and mitogen-activated protein kinase cascades. Neuroscience 156:898–910.

Même W, Calvo C, Froger N, Ezan P, Amigou E, Koulakoff A, Giaume C (2006) Proinflammatory cytokines released from microglia inhibit gap junctions in astrocytes: potentiation by β-amyloid. FASEB J 20:494–496.

Meske V, Hamker U, Albert F, Ohm TG (1998) The effects of β/A4-amyloid and its fragments on calcium homeostasis, glial fibrillary acidic protein and S100β staining, morphology and survival of cultured hippocampal astrocytes. Neuroscience 85:1151–1160.

Moyer JR Jr, Brown TH (1998) Methods for whole-cell recording from visually preselected neurons of perirhinal cortex in brain slices from young and aging rats. J Neurosci Methods 86:35–54.

Mucke L, Masliah E, Yu GQ, Mallory M, Rockenstein EM, Tatsuno G, Hu K, Kholodenko D, Johnson-Wood K, McConlogue L (2000) High-level neuronal expression of Aβ 1–42 in wild-type human amyloid protein precursor transgenic mice: synaptotoxicity without plaque formation. J Neurosci 20:4050–4058.

Nagy JI, Li W, Hertzberg EL, Marotta CA (1996a) Elevated connexin43 immunoreactivity at sites of amyloid plaques in Alzheimer's disease. Brain Res 717:173–178.

Nagy JI, Hossain MZ, Hertzberg EL, Marotta CA (1996b) Induction of connexin43 and gap junctional communication in PC12 cells over-expressing the carboxy terminal region of amyloid precursor protein. J Neurosci Res 44:124–132.

Nagy JI, Dudek FE, Rash JE (2004) Update on connexins and gap junctions in neurons and glia in the mammalian nervous system. Brain Res Brain Res Rev 47:191–215.

Nielsen HM, Veerhuis R, Holmqvist B, Janciauskiene S (2009) Binding and uptake of Aβ1–42 by primary human astrocytes in vitro. Glia 57:978–988.

Nimmerjahn A, Kirchhoff F, Kerr JN, Helmchen F (2004) Sulforhodamine 101 as a specific marker of astroglia in the neocortex *in vivo*. Nat Methods 1:31–37.

O'Mahony D, Rowan D, Feely J, Walsh JB, Coakley D (1994) Primary auditory pathway and reticular activating system dysfunction in Alzheimer's disease. Neurology 44:2089–2094.

Palmer CV, Adams SW, Bourgeois M, Durrant J, Rossi M (1999) Reduction in caregiver-identified problem behaviors in patients with Alzheimer disease post-hearing-aid fitting. J Speech Lang Hear Res 42:312–328.

Parpura-Gill A, Beitz D, Uemura E (1997) The inhibitory effects of β-amyloid on glutamate and glucose uptakes by cultured astrocytes. Brain Res 754:65–71.

Peters O, Schipke CG, Philipps A, Haas B, Pannasch U, Wang LP, Benedetti B, Kingston AE, Kettenmann H (2009) Astrocyte function is modified by Alzheimer's disease-like pathology in aged mice. J Alzheimer's Dis 18:177–189.

Pihlaja R, Koistinaho J, Malm T, Sikkilä H, Vainio S, Koistinaho M (2008) Transplanted astrocytes internalize deposited beta-amyloid peptides in a transgenic mouse model of Alzheimer's disease. Glia 56:154–163.

Puchtler H, Sweat F, Levine M (1962) On the binding of Congo red by amyloid. J Histochem Cytochem 10:355–364.

Puchtler H, Sweat F (1965) Congo red as a stain for fluorescence microscopy of amyloid. J Histochem Cytochem 10:693–694.

Querfurth HW, LaFerla FM (2010) Alzheimer's disease. N Engl J Med. 362:329–344.

Rozental R, Srinivas M, Spray DC (2001) How to close a gap junction channel. Efficacies and potencies of uncoupling agents. Methods Mol Biol 154:447–476.

Simpson JE, Ince PG, Haynes LJ, Theaker R, Gelsthorpe C, Baxter L, Forster G, Lace GL, Shaw PJ, Matthews FE, Savva GM, Brayne C, Wharton SB, MRC Cognitive Function and Ageing Neuropathology Study Group (2010a) Population variation in oxidative stress and astrocyte DNA damage in relation to Alzheimer-type pathology in the ageing brain. Neuropathol Appl Neurobiol 36:25–40.

Simpson JE, Ince PG, Lace G, Forster G, Shaw PJ, Matthews F, Savva G, Brayne C, Wharton SB, MRC Cognitive Function and Ageing Neuropathology Study Group (2010b) Astrocyte phenotype in relation to Alzheimer-type pathology in the ageing brain. Neurobiol Aging 31:578–590.

Sinha UK, Hollen KM, Rodriguez R, Miller CA (1993) Auditory system degeneration in Alzheimer's disease. Neurology 43:779–785.

Sokoloff L, Reivich M, Kennedy C, Des Rosiers MH, Patlak CS, Pettigrew KD, Sakurada O, Shinohara M (1977) The [^{14}C]deoxyglucose method for measurement of local cerebral glucose utilization: theory, procedure, and normal values in conscious and anesthetized rats. J Neurochem 28: 897–916.

Speizer L, Haugland R and Kutchai H (1985) Asymmetric transport of a fluorescent glucose analogue by human erythrocytes. Biochim Biophys Acta 815:75–84.

Thi MM, Urban-Maldonado M, Spray DC, Suadicani SO (2010) Intercellular communication among astrocytes is enhanced by high glucose exposure in culture. 2010 Transactions of the American Society for Neurochemistry, 106.

Weller RO, Subash M, Preston SD, Mazanti I, Carare RO (2008) Perivascular drainage of amyloid-β peptides from the brain and its failure in cerebral amyloid angiopathy and Alzheimer's disease. Brain Pathol 18:253–266.

Wharton SB, O'Callaghan JP, Savva GM, Nicoll JA, Matthews F, Simpson JE, Forster G, Shaw PJ, Brayne C, Ince PG, MRC Cognitive Function and Ageing Neuropathology Study Group (2009) Population variation in glial fibrillary acidic protein levels in brain ageing: relationship to Alzheimer-type pathology and dementia. Dement Geriatr Cogn Disord 27:465–473.

Wilcock DM, Gordon MN, Morgan D (2006) Quantification of cerebral amyloid angiopathy and parenchymal amyloid plaques with Congo red histochemical stain. Nat Protoc 1:1591–1595.

Wyss-Coray T, Loike JD, Brionne TC, Lu E, Anankov R, Yan F, Silverstein SC, Husemann J (2003) Adult mouse astrocytes degrade amyloid-β *in vitro* and *in situ*. Nat Med 9:453–457.

Received 26 May 2010/22 July 2010; accepted 23 July 2010

Published as Immediate Publication 30 July 2010, doi 10.1042/AN20100017